

# MoLingo: Motion–Language Alignment for Text-to-Human Motion Generation

Yannan He<sup>1,2</sup> Garvita Tiwari<sup>1,2,3</sup> Xiaohan Zhang<sup>1,2,3</sup> Pankaj Bora<sup>1</sup>  
Tolga Birdal<sup>4</sup> Jan Eric Lenssen<sup>3</sup> Gerard Pons-Moll<sup>1,2,3</sup>

<sup>1</sup>University of Tübingen, Germany, <sup>2</sup>Tübingen AI Center, Germany,

<sup>3</sup>Max Planck Institute for Informatics, Saarland Informatics Campus, Germany

<sup>4</sup>Imperial College London, United Kingdom

<https://hynann.github.io/molingo/MoLingo.html>

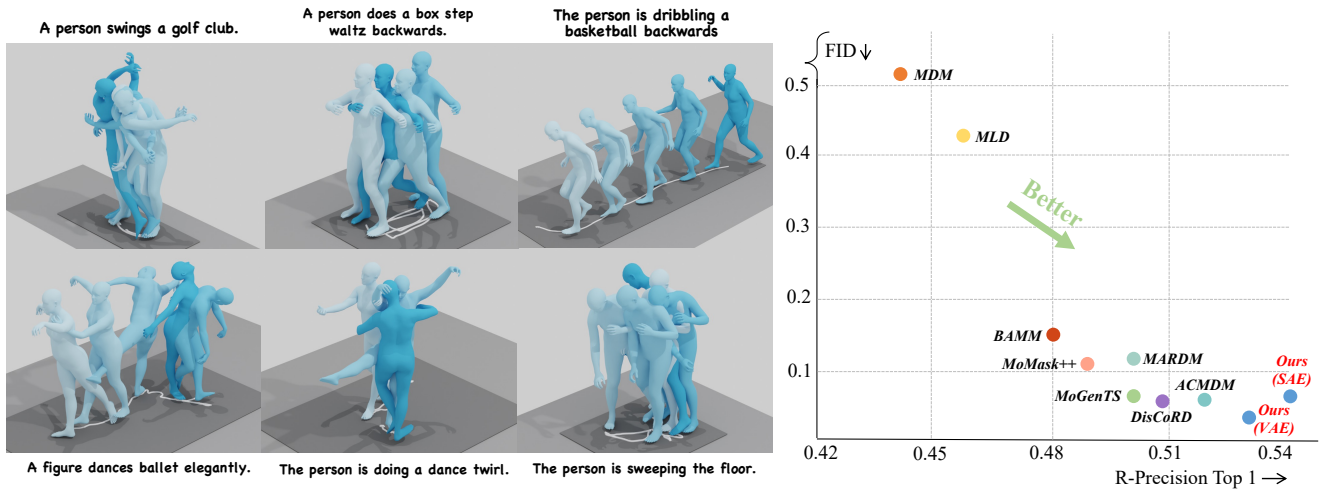


Figure 1. *Left:* Given text prompts, MoLingo generates realistic and text-aligned motions, ranging from daily movements like sweeping to more challenging movements like dancing. *Right:* MoLingo significantly outperforms previous works in both FID and R-Precision scores. The difference can best be seen in motion, hence we urge the reader to view the supplementary video.

## Abstract

We introduce *MoLingo*, a text-to-motion (T2M) model that generates realistic, lifelike human motion by denoising in a continuous latent space. Recent works perform latent space diffusion, either on the whole latent at once or auto-regressively over multiple latents. In this paper, we study how to make diffusion on continuous motion latents work best. We focus on two questions: (1) how to build a semantically aligned latent space so diffusion becomes more effective, and (2) how to best inject text conditioning so the motion follows the description closely. We propose a semantic-aligned motion encoder trained with frame-level text labels so that latents with similar text meaning stay close, which makes the latent space more diffusion-friendly. We also compare single-token conditioning with a multi-token cross-attention scheme and find that cross-attention gives better motion realism and text–motion alignment. With semantically aligned latents, auto-regressive generation, and cross-attention text conditioning, our model sets a new state

of the art in human motion generation on standard metrics and in a user study. We will release our code and models for further research and downstream usage.

## 1. Introduction

Generating realistic human motion from text is crucial for computer animation, AR/VR entertainment, and building agents that can follow human instructions. In recent years, text-labeled human motion datasets [16, 47] have kicked off this research area, and diffusion-based generative models have brought a major improvement in generated motion quality. Earlier text-to-motion (T2M) works used diffusion models to denoise motion directly in pose space [4, 8, 13, 22, 26, 29, 31, 53, 67, 68, 75] and achieved good performance. However, denoising raw pose frames is hard because the joint distribution is very complex, and it can also bring artifacts by preserving mocap noise [37]. To address this, recent

works first encode motion into a compact latent space [6, 9, 10, 72, 73], then run diffusion in that space, and finally decode it back to motion. Current methods mainly follow two tracks: (1) diffusion on the whole latent space at once [6, 9, 10, 25], and (2) split the sequence into multiple latents and denoise them auto-regressively [39, 55, 62, 74, 76].

In this work, we investigate how to most effectively perform text-to-motion diffusion in a continuous latent space. There are two key questions here: (1) what makes a good latent space for motion diffusion, and (2) how to inject the text condition most effectively.

For the first question, we study motion latent spaces w.r.t. latent size and semantic alignment, motivated by recent latent space studies for image generation [28, 61, 63]. Specifically, we introduce a semantically aligned motion encoder that preserves key temporal structure and pulls atomic motion latents with similar text semantics closer in the latent space. We additionally use frame-level text labels guiding how motion latents are distributed. Altogether results in a model which can follow the text instructions more faithfully.

For text conditioning, recent works usually either attach a single text token to the motion latents [6, 18, 44, 45, 53, 66], or use that token to modulate the transformer-based diffusion backbone [39, 40]. Our experiments show that a single token is not expressive enough. Instead, we employ multiple text tokens with cross-attention to the motion latents. This results in stronger conditioning.

Based on these insights, we introduce MoLingo, a masked auto-regressive rectified-flow model that combines semantically aligned latent spaces with multi-token cross-attention. MoLingo generates human motion that is both natural and faithful to text instructions, achieving state-of-the-art results in FID, R-Precision, and a user study, including challenging motions such as dancing Fig. 1 (please see the video too).

In summary, our **contributions** are:

- We introduce **MoLingo**, setting the new state of the art in human motion generation using masked auto-regressive rectified flow on a continuous latent space to produce natural and realistic motions.
- We propose two variants of our model: one with a semantically aligned latent space of text and motion and one with a plain VAE. We show that alignment helps the model to faithfully follow the text instruction.
- Instead of conditioning on text based on a single token (common), we find that multiple tokens and cross-attention with motion latents yields significant improvement.

We will make our code and models publicly available for further research and downstream usage.

## 2. Related Work

Human motion is a vastly studied topic. Different from unconditional generation [32, 51, 64], here we review recent advances in text-driven 3D human motion generation, cate-

gorized into: human motion generation, evaluation protocols, and representation learning for diffusion models.

**Human motion generation.** Human motions can be parameterized either continuously or discretely. For continuous representations, diffusion-based methods generate motions either directly in the pose-frame space [4, 5, 8, 26, 29, 31, 43, 52, 53, 67–70, 75] or in a learned latent space [6, 9, 10, 39, 40, 55, 62, 72, 73]. While diffusion-based approaches can produce diverse and realistic motions, methods that generating in the pose-frame space suffer from the noise present in mocap-based datasets [37], leading to artifacts in generated motions. Latent space diffusion models alleviate the issue by first compressing motions into a compact latent space. However, encoding an entire sequence into a single latent vector [6, 9, 10, 25] can lose important temporal details and fine-grained motion cues. Vector-quantization (VQ)-based next-token prediction methods [3, 14, 17–19, 21, 23, 24, 33, 44–46, 58, 60, 66, 71] first discretize continuous motions into a series of codebook tokens, then use auto-regressive transformers to predict subsequent token entry conditioned on text, treating motion as a foreign language. While this discretization preserves more temporal information from the input motion and makes training easier via cross-entropy, mapping continuous motion to a finite codebook still introduces quantization error. This reduces fine-grained details and realism, especially for challenging or fast motions. More recently, inspired by advances in image generation [30], several works [39, 55, 62, 76] have adopted continuous-valued latents for diffusion-based auto-regressive motion generation, improving motion quality and reducing the reconstruction artifacts of VQ-based methods. We follow this line, but introduce with a stronger text-conditioning mechanism and a semantically aligned latent space, which together enable state-of-the-art motion generation performance.

**Motion parameterization and evaluation protocols.** Human motion is naturally represented as a sequence of pose frames. Both, how we parameterize the pose configuration and how we quantify motion quality, are crucial for assessing realism and semantic faithfulness. FID [20] is the most widely used metric to measure realism and diversity for generative models. To better align with human perception, recent works explore predicting of human preference scores directly [57, 59]. In this context, HumanML3D [16] introduced a 263-dimensional motion representation together with a motion feature extractor for computing metrics such as FID. In addition to rotations, this representation also contains joint positions, velocities, and foot-contact signals, which serve as extra regularization. This Guo-263 protocol enabled robust comparison for a wide range of text-to-motion works [6, 18, 53, 66, 67], but subsequent studies have revealed limitations [1, 29, 39, 42, 43, 62]. (1) [39] pointed out that the 263D representation is redundant. They keep only the

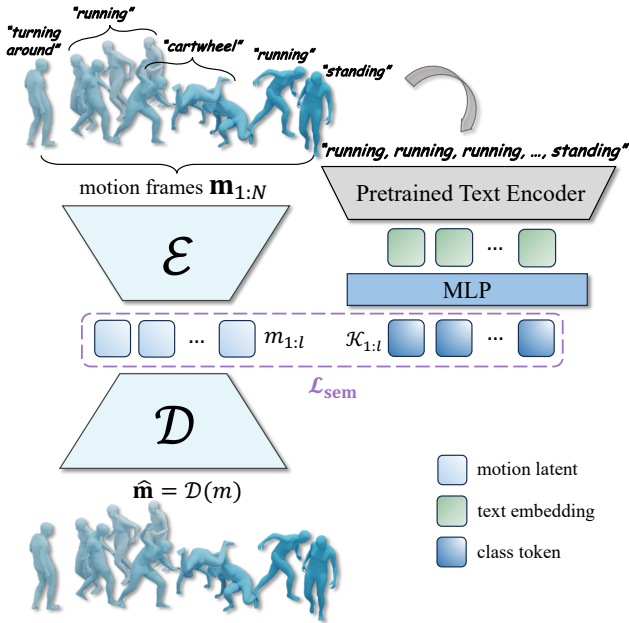


Figure 2. **Semantically aligned autoencoder architecture.** The model comprises an encoder–decoder autoencoder for motion sequences and a parallel text-encoding branch that maps frame-level text labels into class tokens. A cosine-similarity loss  $\mathcal{L}_{\text{sem}}$  is applied to align the motion latents with their corresponding class tokens.

first 67 dimensions, corresponding to the pelvis trajectory and local joint positions, resulting in the MARDM-67 protocol. (2) [62] pointed out that the rotation components in Guo-protocol are derived via inverse kinematics (IK), which introduces errors. They rebuilt the representation into 272 dimensions by taking rotations directly from AMASS [37], thereby avoiding IK artifacts. They further adopt a better-designed cross-modal embedding space, TMR [42], which provides a more semantically coherent latent space for evaluation, resulting in the MS-272 protocol. Recent works have reported FID using TMR evaluator [19, 29, 43, 62]. For the standard 263-dimensional representation, we also employ the TMR evaluator on the original 263D representation, referred to as TMR-263. Together with MARDM-67, we report results across all these evaluators to ensure a fair and comprehensive evaluation.

**Representation learning for diffusion models.** Learning effective latent representations is crucial for high-quality generation with latent diffusion models. Recent works have focused on discovering latent spaces suitable to diffusion, exploring what constitutes a “diffusible” representation. REPA [63] introduces an approach that aligns noisy input states in diffusion models with representations from pre-trained visual encoders. REPA-E [28] proposes to train the diffusion model and its VAE tokenizer end-to-end, achieving stable and effective joint training of both components. REG [61] proposes to entangle low-level image latents with a single high-level class token from pre-trained foundation mod-

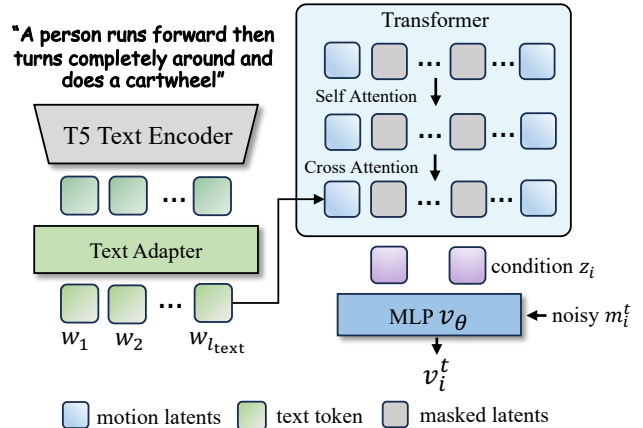


Figure 3. **Auto-regressive flow-based latent denoising.** Our generation model uses a standard transformer decoder to obtain conditioning vectors  $z$ , which guides an MLP in iteratively refining latents. During training the motion latents are randomly masked and replaced with learnable tokens. During inference, we initialize with **fully masked latents**, iteratively denoise them, and decode the final latents to obtain the generated motion.

els, enhancing global control for the denoising process. [27] integrates masked autoencoders into the diffusion framework, while recent work has also explored semantic regularization losses [41] to improve latent space structure. Motivated by these insights, we investigate how to enrich motion latent spaces with semantic information to facilitate the diffusion process and improve generation quality.

### 3. Method

In this section, we introduce our method for realistic human motion generation. We start by giving an overview of the solved task and our method.

**Human motion generation task.** We aim to generate a sequence  $\mathbf{m}_{1:N}$  of 3D human motion with length  $N$ , where each  $\mathbf{m}_i \in \mathbb{R}^D$  represents a human pose configuration. The generation process is conditioned on a textual description  $c$ .

**Method overview.** As illustrated in Fig. 2 and Fig. 3, our approach consists of two key components: (1) a motion encoder that maps motion sequences to semantically aligned continuous-valued motion latents (Sec. 3.1) and (2) a masked auto-regressive transformer with rectified flow [34] output heads, progressively denoising these latents (Sec. 3.2). Similar to [39, 62], we perform auto-regressive generation directly in the continuous domain using a flow-based objective, which avoids poor reconstruction performance observed in earlier methods [18, 24, 44, 45, 66].

#### 3.1. Encoding Motions into Latents

We consider three variants of motion autoencoders: a variational autoencoder (VAE), a vanilla autoencoder (AE), and we further propose a semantically aligned autoencoder (SAE). Since our encoder–decoder is built with 1D temporal

Table 1. **Quantitative results on the MARDM-67 evaluator.** We compare our method with a broad set of motion generation approaches, from early models [6, 53] to recent ones [19, 40], covering pose-frame diffusion [53], single-vector latent diffusion [6, 9], VQ-based next-token prediction [7, 18, 19, 44, 45, 65], and continuous-valued auto-regressive models [39, 40]. We report the mean results over 20 independent runs, and the  $\pm$  values indicate the 95% confidence interval. Our method achieves state-of-the-art FID, R-Precision, and CLIP-Score. Green cells highlight the best scores, and yellow cells the second best.

Methods	FID $\downarrow$	R-Precision			CLIP-Score $\uparrow$	MModality $\uparrow$
		Top 1 $\uparrow$	Top 2 $\uparrow$	Top 3 $\uparrow$		
Real	0.000 $\pm$ .000	0.503 $\pm$ .002	0.696 $\pm$ .001	0.795 $\pm$ .002	0.639 $\pm$ .001	-
MDM-50Step [53]	0.518 $\pm$ .032	0.440 $\pm$ .007	0.636 $\pm$ .006	0.742 $\pm$ .004	0.578 $\pm$ .003	3.604 $\pm$ .031
MLD [6]	0.431 $\pm$ .014	0.461 $\pm$ .004	0.651 $\pm$ .004	0.750 $\pm$ .003	0.610 $\pm$ .003	3.506 $\pm$ .031
MoMask [18]	0.116 $\pm$ .006	0.490 $\pm$ .004	0.687 $\pm$ .003	0.786 $\pm$ .003	0.637 $\pm$ .003	1.309 $\pm$ .058
MMM [45]	0.132 $\pm$ .004	0.487 $\pm$ .003	0.683 $\pm$ .002	0.782 $\pm$ .001	0.635 $\pm$ .003	1.455 $\pm$ .106
BAMM [44]	0.147 $\pm$ .005	0.480 $\pm$ .003	0.671 $\pm$ .003	0.772 $\pm$ .003	0.630 $\pm$ .001	1.954 $\pm$ .070
MogenTS [65]	0.060 $\pm$ .004	0.500 $\pm$ .003	0.694 $\pm$ .002	0.793 $\pm$ .002	0.636 $\pm$ .001	0.882 $\pm$ .032
MLD++ [9]	2.027 $\pm$ .021	0.500 $\pm$ .003	0.691 $\pm$ .002	0.789 $\pm$ .001	0.639 $\pm$ .002	1.924 $\pm$ .065
MotionLCM-V2 [9]	2.267 $\pm$ .023	0.501 $\pm$ .002	0.693 $\pm$ .002	0.790 $\pm$ .002	0.640 $\pm$ .003	1.780 $\pm$ .062
DisCoRD [7]	0.053 $\pm$ .004	0.506 $\pm$ .003	0.699 $\pm$ .003	0.796 $\pm$ .003	0.645 $\pm$ .001	1.303 $\pm$ .047
MARDM-v [39]	0.114 $\pm$ .007	0.500 $\pm$ .004	0.695 $\pm$ .003	0.795 $\pm$ .003	0.642 $\pm$ .002	2.231 $\pm$ .071
ACMDM-S-PS22 [40]	0.109 $\pm$ .005	0.508 $\pm$ .002	0.701 $\pm$ .003	0.798 $\pm$ .003	0.642 $\pm$ .001	2.156 $\pm$ .061
ACMDM-XL-PS2 [40]	0.058 $\pm$ .004	0.522 $\pm$ .002	0.713 $\pm$ .003	0.807 $\pm$ .002	0.652 $\pm$ .001	2.077 $\pm$ .083
MoMask++ [19]	0.108 $\pm$ .007	0.492 $\pm$ .003	0.683 $\pm$ .003	0.782 $\pm$ .002	0.634 $\pm$ .001	1.259 $\pm$ .054
MoLingo (VAE)	0.049 $\pm$ .003	0.528 $\pm$ .002	0.721 $\pm$ .002	0.815 $\pm$ .002	0.672 $\pm$ .001	2.307 $\pm$ .049
MoLingo (SAE)	0.064 $\pm$ .002	0.542 $\pm$ .002	0.739 $\pm$ .002	0.832 $\pm$ .002	0.686 $\pm$ .001	2.215 $\pm$ .063

convolutions, the sequential structure of the input motion is preserved by encoding  $N$  motion frames into  $l = N/h$  latents, resulting in motion latents  $m_{1:l} \in \mathbb{R}^{l \times d}$ , where  $d$  is the latent dimension. In practice, we adopt a causal architecture [62] where both the motion encoder and decoder consist of stacked 1D convolutional layers.

**Semantically aligned autoencoder (SAE).** We introduce a continuous-valued autoencoder that preserves fine-grained human motion details while maintaining semantic for each latent, as shown in Fig. 2. To obtain a more structured motion latent space with rich semantics, we encourage motion latents corresponding to similar semantics to be close in the latent space. In practice, we use the BABEL dataset [48], which provides frame-level textual label annotations for each motion sequence. For each motion latent  $m_j$ , we collect the text labels from the motion frames temporally aligned with that latent, encode them using a frozen text encoder, average the resulting embeddings, and apply a linear projection to match the motion latent dimension, getting the class token  $\kappa_j$ . We then treat these class tokens as the teacher to guide the motion latent distribution. For each training batch, we apply a cosine similarity loss to encourage closer alignment between motion latents and their corresponding class tokens. However, since BABEL contains highly repetitive frame-level annotations, consecutive motion latents may be assigned an identical class token, leading to overly strong or incorrect alignment. To address this, we first compute a similarity score between consecutive class tokens:

$\Delta_i = \langle \kappa_i, \kappa_{i+1} \rangle, 1 \leq i < B, B = b \times l$ , and discard class tokens and their corresponding motion latents whose  $\Delta_i$  exceeds a threshold  $\tau$ , resulting in the filtered index set  $\mathcal{I}$ . Here  $\langle \cdot, \cdot \rangle$  denotes the cosine similarity, and  $b$  is the batch size. We then minimize the semantic loss from the text-induced distribution to the motion-induced one:

$$\mathcal{L}_{\text{sem}} = \frac{1}{|\mathcal{I}|} \sum_{i \in \mathcal{I}} \left( 1 - \frac{m_i \cdot \kappa_i}{\|m_i\| \|\kappa_i\|} \right) \quad (1)$$

**Training objective.** First, the SAE is trained to preserve motion reconstruction quality via a reconstruction loss:

$$\mathcal{L}_{\text{recon}} = \mathcal{L}_{\text{feat}} + \lambda_{\text{joint}} \mathcal{L}_{\text{joint}} + \lambda_{\text{vel}} \mathcal{L}_{\text{vel}} \quad (2)$$

where,

$$\mathcal{L}_{\text{feat}} = \|\mathbf{m} - \mathcal{D}(m)\|_2^2 \quad \mathcal{L}_{\text{joint}} = \|\mathcal{T}(\mathbf{m}) - \mathcal{T}(\mathcal{D}(m))\|_2^2 \quad (3)$$

$$\mathcal{L}_{\text{vel}} = \frac{1}{N-1} \sum_{n=1}^{N-1} \left\| \left( \mathcal{T}(\mathbf{m})_{n+1} - \mathcal{T}(\mathbf{m})_n \right) - \left( \mathcal{T}(\mathcal{D}(m))_{n+1} - \mathcal{T}(\mathcal{D}(m))_n \right) \right\|_2^2 \quad (4)$$

where  $\mathcal{T}$  represents the function that transforms motion representation to body joint positions. These terms respectively penalize differences in motion representations, joint positions and joint velocities. The final loss is:

$$\mathcal{L}_{\text{SAE}} = \mathcal{L}_{\text{recon}} + \lambda_{\text{sem}} \mathcal{L}_{\text{sem}} + \lambda_{\text{KL}} \mathcal{L}_{\text{KL}} \quad (5)$$



Table 2. **Ablation studies.** We analyze: (1) different text-conditioning mechanisms, and (2) the effect of using a semantically aligned latent space. **AdaLN** denotes single-text-token conditioning with DiT-style modulation; note that the first row corresponds to MARDM [39]. **CrossAttn** denotes multi-token cross-attention conditioning. We conduct all experiments using the MARDM-67 evaluator with 4x downsampling and latent dimensions of 16. We adopt adapter depth 6 for T5+CrossAttn setting.

Conditioning Mechanism	Text Encoder	Autoencoder Type	FID ↓	R-Precision			CLIP-Score ↑
				Top 1 ↑	Top 2 ↑	Top 3 ↑	
AdaLN	CLIP T5	AE	0.114±.007	0.500±.004	0.695±.003	0.795±.003	0.642±.002
			0.077±.004	0.508±.003	0.700±.003	0.795±.002	0.650±.001
CrossAttn	T5	VAE	0.049±.003	0.528±.002	0.721±.002	0.815±.002	0.672±.001
		AE	0.051±.002	0.533±.003	0.727±.003	0.820±.002	0.673±.001
		SAE	0.064±.002	0.542±.002	0.739±.002	0.832±.002	0.686±.001

with  $\mathcal{L}_{\text{KL}} = D_{\text{KL}}(q(m|\mathbf{m}) \parallel p(m))$  is the KL Divergence. Please refer to the appendix for more details.

### 3.2. Masked Auto-regressive Motion Generation

**Input preparation.** As shown in Fig. 3, after encoding the input motions into latents  $m_{1:l}$ , we first encode the prompt  $c$  using a frozen T5-Large [50] text encoder. To further enhance cross-modal interaction for the subsequent cross-attention, we pass the text embeddings through a text adapter consisting of  $l_{\text{adapter}}$  transformer encoder blocks, obtaining the final text representation  $\mathbf{w} = \{w_1, w_2, \dots, w_{l_{\text{text}}}\}$ . We then randomly select a subset of motion latents in  $m_{1:l}$ , and replace them with a learnable mask latent during training. We continue to denote the masked latent sequence as  $m_{1:l}$  for simplicity.  $\mathbf{w}$  and  $m_{1:l}$  then serve as the inputs to the subsequent auto-regressive denoising stage.

**Auto-regressive flow-based latent denoising.** Given the masked sequence of latents  $m_{1:l}$ , we decompose the joint distribution over all latents using the chain rule of probability:

$$p(m_1, \dots, m_l) = \prod_{i=1}^l p(m_i | c, m_1, \dots, m_{i-1}), \quad (6)$$

and generate a motion sequence by iteratively sampling latents followed by decoding with  $\mathcal{D}$ . Each step uses a transformer-based network to sample from the conditional probability  $p(m_i | c, m_1, \dots, m_{i-1})$  walking through a reverse ODE trajectory. In practice, we use rectified flow [34] as our flow-based model. To combine the strengths of auto-regression and rectified flow, following [12, 30], we use a standard decoder-only transformer model  $\Phi$  to obtain a conditioning vector  $z_i = \Phi(w_1, \dots, w_{l_{\text{text}}}; m_1, \dots, m_{i-1})$ . Each transformer block consists of self-attention, cross-attention and MLP layers. The self attention and MLP layer operate only on the motion latents  $m_{1:l}$ , for cross attention, output of the self attention serve as the queries and text tokens  $\mathbf{w}$  as keys and values. Then we feed  $z_i$  into an MLP  $v_\theta$  to approximate the reverse distribution:

$$\mathcal{L}(z_i, m_i) = \mathbb{E}_{m_i, \epsilon, t} [\|v_\theta(m_i^t, t, z_i) - \dot{\alpha}_t m_i - \dot{\sigma}_t \epsilon\|^2], \quad (7)$$

where the noisy  $m_i^t$  is obtained by linearly interpolating between the Gaussian noise  $\epsilon$  and the clean latent:  $m_i^t = \alpha_t m_i + \sigma_t \epsilon$ ,  $\epsilon \sim \mathcal{N}(0, \mathbf{I})$  with  $\alpha_t$  a decreasing and  $\sigma_t$  an increasing function of time  $t$ . During training, we use bidirectional attention so that masked latents can attend to all unmasked latents, and unmasked latents can also see each other.

**Inference.** We initialize all motion latents with the learned mask latent at the start of inference. We then iteratively select one or a subset of latent positions, run the transformer once to obtain the corresponding conditioning vector(s)  $z$ , and feed  $z$  into the MLP to perform the reverse flow-based sampling at those positions, replacing the masked latents with clean ones. This process is repeated until all motion latents are clean. We finally pass the clean latent sequence to the motion decoder  $\mathcal{D}$  to produce the generated motion.

## 4. Experiments

In this section, we first present the experimental setup in Sec. 4.1, followed by ablation studies in Sec. 4.2, qualitative and quantitative comparisons with state-of-the-art methods in Sec. 4.3. To better reflect human perception, we also conduct user studies, reported in Sec. 4.3.

### 4.1. Setup

**Implementation details.** Our models are implemented in PyTorch. To ensure a fair comparison with state-of-the-art human motion generation methods, we use the HumanML3D [16] dataset for training and evaluation. HumanML3D sources motions from AMASS [37] and HumanAct12 [15] and provides two to three manual text annotations per motion. The full dataset consists of 29,024 motions and 87,834 text descriptions. All motions are unified to 20 FPS and last up to 10 seconds. We further use the 272-dimensional 30 FPS version of HumanML3D to train the model for comparison with [62]. For SAE training, we use the intersection between BABEL [48] and HumanML3D to apply the semantic loss, and then use the full dataset to apply the remaining losses. We train the motion autoencoders with

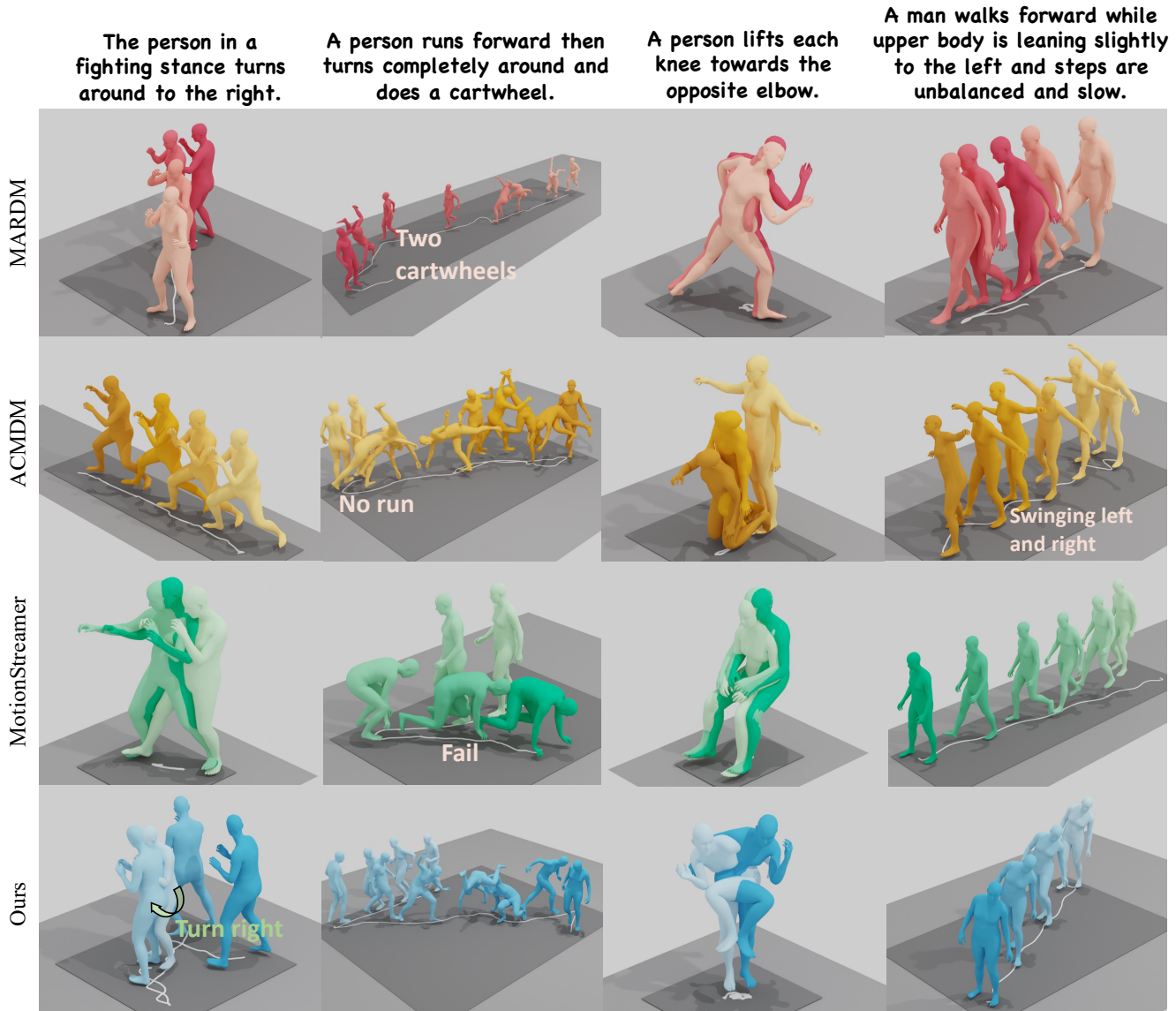


Figure 4. **Qualitative comparisons** with MARDM [39], ACMDM [40], and MotionStreamer [62]. The color transitions from light to dark to indicate temporal flow. Our method generates more natural and text-aligned motions, ranging from everyday movements to challenging scenarios like cartwheel. In contrast, other methods either fail to follow fine-grained text instructions (e.g., *run first, then turn around, then do a cartwheel*, or *leaning left while walking*), or collapse completely (e.g., knees touching elbows). Our method follows the specified action order while preserving realism. For methods using the MARDM-67 representation [39, 40], we employ Simplify [2] to convert their outputs to SMPL [35] meshes. We refer readers to the supplementary videos for more detailed visualizations of dynamic motions.

a batch size of 256 for 5000 epochs, using a learning rate of  $5 \times 10^{-5}$ . For our auto-regressive latent rectified flow model, we train for about 800 epochs with a batch size of 256. The learning rate warms up linearly for the first 100 epochs and then remains constant at  $8 \times 10^{-4}$ . We apply Exponential Moving Average (EMA) to stabilize training. The model is trained with classifier-free guidance (CFG) by replacing 10% of the text prompts into the same null prompt, and at inference time we sample latents with a CFG scale of 6.0. The entire training process for our best model configuration

in Tab. 1 takes approximately 10 hours with four Nvidia H100 GPUs. Please refer to the supplementary document for further details such as hyperparameter setting, inference speed, etc.

**Evaluation protocol.** To enable a more comprehensive evaluation, we report metrics using MARDM-67 as our main benchmark, which enables us to compare with the most broad range of works, including [39, 40]. Since some other works built on other representations (e.g. 272D), for a fair comparison with methods built on alternative motion repre-

Table 3. **Performance under different SAE configurations.** We ablate three design choices for SAE: (1) the semantic regularization loss (cosine similarity vs. InfoNCE), (2) whether KL divergence is applied jointly, and (3) the weight of  $\mathcal{L}_{\text{sem}}$ . The configuration with cosine similarity, KL divergence, and a relatively small weight (0.001) gives the best SAE design, significantly improving text–motion alignment (R-Precision and CLIP-score) while maintaining FID comparable to SOTA models.

semantic regularization	KL	$\lambda_{\text{sem}}$	FID ↓	R-Precision ↑			CLIP-Score ↑
				Top 1	Top 2	Top 3	
Cosine	✗	0.1	0.083 $\pm$ .003	0.527 $\pm$ .002	0.719 $\pm$ .002	0.817 $\pm$ .002	0.671 $\pm$ .001
	✓	0.1	0.071 $\pm$ .003	0.518 $\pm$ .002	0.712 $\pm$ .002	0.808 $\pm$ .002	0.667 $\pm$ .001
	✗	0.01	0.081 $\pm$ .003	0.529 $\pm$ .002	0.720 $\pm$ .002	0.822 $\pm$ .002	0.672 $\pm$ .001
	✓	0.01	0.074 $\pm$ .003	0.524 $\pm$ .002	0.722 $\pm$ .002	0.819 $\pm$ .002	0.673 $\pm$ .001
	✗	0.001	0.062 $\pm$ .003	0.535 $\pm$ .002	0.731 $\pm$ .002	0.826 $\pm$ .002	0.680 $\pm$ .001
	✓	0.001	0.064 $\pm$ .002	0.542 $\pm$ .002	0.739 $\pm$ .002	0.832 $\pm$ .002	0.686 $\pm$ .001
InfoNCE	✗	0.001	0.129 $\pm$ .007	0.523 $\pm$ .002	0.721 $\pm$ .002	0.813 $\pm$ .002	0.671 $\pm$ .001

sentations, we additionally evaluate under their corresponding protocol MS-272. Furthermore, to pioneering a more robust evaluation benchmark for the future research, we for the first time give a most number of previous works and our work on TMR-263 evaluator. Specifically, we report a set of metrics under different evaluators. We use **FID** to measure the distance between the generated and real motion distributions, **R-Precision** and **CLIP Score** to assess text–motion alignment, and **MModality** to quantify the diversity of motions generated from the same textual description.

## 4.2. Ablation Studies

We provide a comprehensive ablation on different text-conditioning mechanisms, autoencoder variants followed by an analysis of the effects of different latent sizes in Fig. 5.

**Text condition mechanism.** Tab. 2 uses MARDM [39] (row 1) as the baseline to demonstrate the effectiveness of our design choices. We observe that using T5 achieves better performance even without multi-text-token cross attention (row 2), indicating the text encoder plays a key role in preserving rich semantics. Our multi-token cross attention design achieves clearly better text-motion alignment while achieving lower FID, suggesting that leveraging the full set of text tokens is more expressive.

**Effect of SAE.** As shown in Tab. 2, the proposed SAE clearly outperforms both the vanilla AE and the VAE. It consistently achieves the best text–motion alignment scores while maintaining a comparable FID to SOTA models, indicating that enforcing semantic alignment yields a more semantically rich latent space that benefits text–motion alignment. We further investigate different forms of semantic regularization and the influence of the weighting factor  $\lambda_{\text{sem}}$  in Tab. 3. The variant that incorporates KL-divergence-based supervision with a small weighting factor achieves the best performance. For the semantic regularization strategy, we also compare against InfoNCE supervision, a common choice in contrastive learning [42], but it gives worse results. InfoNCE imposes a hard contrastive constraint that not only

pulls together motion latents sharing the same label, but also explicitly pushes apart latents associated with different labels. However, as discussed in Sec. 3.1, the available text labels lack diversity: semantically similar motions might all be mapped to the same label. However, human motion is continuous and ambiguous, and a motion latent corresponding to one label may also share properties with another category. Therefore, InfoNCE applies an overly rigid constraint, forcing each motion latent to align exactly with a fixed class token. In contrast, our method employs a soft cosine-similarity loss that only encourages positive text–motion pairs to move closer, while preserving the unique characteristics of each latent. This softer regularization achieves better quantitative results and leads to a more semantically meaningful and well-separated latent space.

**Exploration with the latent size.** There are two key factors that determine the size of our motion latent space: (1) the number of latents, and (2) the dimensionality of each latent. Fig. 5 presents a comprehensive ablation over both aspects. We observe that increasing the number of latents, i.e., moving from 4 $\times$  to 2 $\times$  compression, leads to consistently better R-Precision scores, indicating stronger text–motion alignment due to the preservation of more fine-grained motion details. In contrast, increasing the latent dimensionality has a negative effect on overall performance.

## 4.3. Comparison with SOTA Methods

We finally select the model using auto-regressive generation with T5 + CrossAttn conditioning, at 4 $\times$  temporal down-sampling and a 16-d latent space, as our best configuration. We choose two variants with VAE and SAE respectively. In this section, we present qualitative comparisons, quantitative results, and a user study.

**Qualitative comparison.** Fig. 4 shows qualitative comparisons with MARDM [39], ACMDM [40] and Motion-Streamer [62]. Our method generates more realistic motions, even for challenging cases like cartwheels and elbow touching knees. As static figures cannot fully capture motion dif-

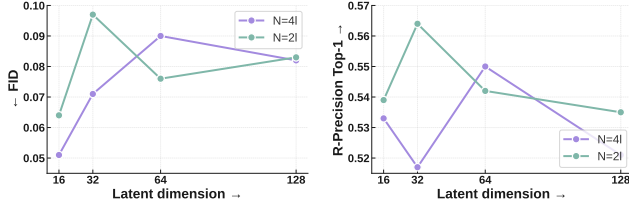


Figure 5. **Effect of latent dimension and temporal downsampling.** We vary the latent dimension (16–128) under two temporal compression settings: (4×) and (2×). Overall, the 4× setting gives comparable or better performance than 2×, showing that is beneficial that a single latent encodes 4 frame, even 2× preserves more fine-grained temporal information.

ferences, we recommend viewing the supplementary videos for a better comparison.

### Quantitative comparison using MARDM-67 protocol.

We present the comparison in Tab. 1. Our approach outperforms prior methods in both distributional quality and text–motion faithfulness, reducing FID from 0.053 to 0.049 for our VAE variant and improving R-Precision (Top-1) from 0.522 to 0.542 for our SAE variant. All results are computed on the HumanML3D test set over 20 generation runs, and we report the mean along with the 95% confidence intervals, ensuring the robustness, motion realism, and semantic faithfulness of our method. For results under other evaluation protocols, we refer readers to the supp. material.

**User study.** We conducted a user study to evaluate the perceptual quality and text–motion alignment of our generated results. We compare our method against three prior works: the VQ-based methods MoMask [18] and DisCoRD [7], and the auto-regressive continuous-space model MotionStreamer [62]. We randomly selected 20 pairs of sequences per baseline. To reduce potential bias, the order of the placement of methods were randomized. Participants were instructed to evaluate the realism and text–motion alignment of the generated motions. For each comparison, we collected responses from 15 users. Please refer to the supplementary material for details of the user study interface. Participants preferred our method over DisCoRD in 83.75% of cases, over MoMask [18] in 77.70% of cases, and over MotionStreamer in 84.70% of cases. These findings indicate that users consistently perceived our generated motions as more realistic than those of prior works. We generate our results using a 272D representation when comparing with MotionStreamer, and a 263D representation when comparing with the other methods, ensuring there are no confounding factors arising from the choice of motion representation.

**Transfer to human robots.** A main application generative human motion models is to transfer motion to robots. To demonstrate the realism of our method, we show that we can directly use a pre-trained controller with physical constraints to transfer our generations to physics simulation. We compare our method to the MotionStreamer on these tasks see

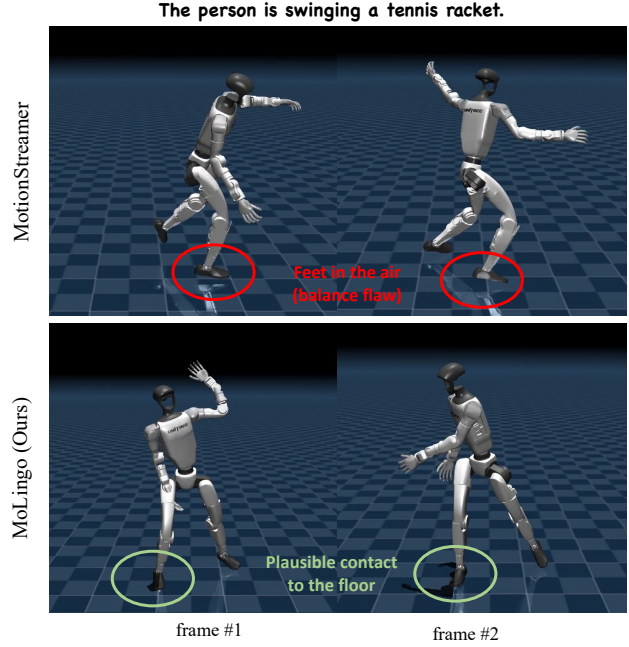


Figure 6. **Incorporating MoLingo with RL Tracking Controller** Our method produces motion with consistently realistic foot–ground interaction across the entire sequence. In contrast, MotionStreamer frequently exhibits balance artifacts. By leveraging MoLingo within the RL tracking controller, our results maintain stable, physically plausible floor contact, leading to more balanced, grounded, and visually convincing character motion. This improved contact behavior also reduces foot sliding and penetration, highlighting the advantage of our approach in capturing physically coherent movement.

Fig. 6. The qualitative and quantitative superiority of our method is also reflected in this task.

## 5. Conclusion and Limitation

In this work, we present MoLingo, a text-to-motion generation model that performs masked auto-regressive rectified flow in a continuous motion latent space aligned with text. By exploring a more structured latent space and a better text condition mechanism, our method produces natural, smooth motions that better follow the input descriptions and achieves state-of-the-art results on a series of evaluators in terms of FID, R-Precision, and CLIP-based scores. A key finding is that aligning the motion latents with text makes the latent space much more aligned with the semantic structure of text models such improves text–motion alignment a lot while preserving good motion quality. We also showed that using multiple text tokens with cross-attention gives stronger text conditioning than a single token, leading to more accurate and realistic generated motions.

**Limitations.** Since our focus is on main body dynamics, our approach does not generate full-body motion with detailed hand movements, an essential aspect of human motion. We see this as an exciting future direction.



**Acknowledgments:** We thank Chuqiao Li and István Sáránci for their helpful discussions and proofreading. We also thank Junyu Zhang for valuable discussions regarding the G1 policy training. The project was made possible by funding from the Carl Zeiss Foundation. This work is supported by the Deutsche Forschungsgemeinschaft (DFG, German Research Foundation) - 409792180 (Emmy Noether Programme, project: Real Virtual Humans) and the German Federal Ministry of Education and Research (BMBF): Tübingen AI Center, FKZ: 01IS18039A. JEL is supported by the German Research Foundation (DFG) - 556415750 (Emmy Noether Programme, project: Spatial Modeling and Reasoning). GPM is a member of the Machine Learning Cluster of Excellence, EXC number 2064/1 - Project number 390727645. This work was supported by the Engineering and Physical Sciences Research Council [grant number EP/X011364/1]. T. B. was supported by a UKRI Future Leaders Fellowship (MR/Y018818/1) as well as a Royal Society Research Grant (RG/R1/241402).

## References

- [1] Léore Bensabath, Mathis Petrovich, and Gül Varol. TMR++: A cross-dataset study for text-based 3d human motion retrieval. In *CVPR Workshop on Human Motion Generation*, 2024. 2
- [2] Federica Bogo, Angjoo Kanazawa, Christoph Lassner, Peter Gehler, Javier Romero, and Michael J Black. Keep it smpl: Automatic estimation of 3d human pose and shape from a single image. In *European conference on computer vision*, pages 561–578. Springer, 2016. 6
- [3] Changan Chen, Juze Zhang, Shrinidhi K Lakshmikanth, Yusu Fang, Ruizhi Shao, Gordon Wetzstein, Li Fei-Fei, and Ehsan Adeli. The language of motion: Unifying verbal and non-verbal language of 3d human motion. In *Proceedings of the Computer Vision and Pattern Recognition Conference*, pages 6200–6211, 2025. 2
- [4] Rui Chen, Mingyi Shi, Shaoli Huang, Ping Tan, Taku Komura, and Xuelin Chen. Taming diffusion probabilistic models for character control. In *ACM SIGGRAPH 2024 Conference Papers*, New York, NY, USA, 2024. Association for Computing Machinery. 1, 2
- [5] Wenshuo Chen, Haozhe Jia, Songning Lai, Keming Wu, Hongru Xiao, Lijie Hu, and Yutao Yue. Free-t2m: Frequency enhanced text-to-motion diffusion model with consistency loss. *arXiv preprint arXiv:2501.18232*, 2025. 2
- [6] Xin Chen, Biao Jiang, Wen Liu, Zilong Huang, Bin Fu, Tao Chen, and Gang Yu. Executing your commands via motion diffusion in latent space. In *Proceedings of the IEEE/CVF Conference on Computer Vision and Pattern Recognition*, pages 18000–18010, 2023. 2, 4, 3
- [7] Jungbin Cho, Junwan Kim, Jisoo Kim, Minseo Kim, Mingyu Kang, Sungeun Hong, Tae-Hyun Oh, and Youngjae Yu. Discord: Discrete tokens to continuous motion via rectified flow decoding. *arXiv preprint arXiv:2411.19527*, 2024. 4, 8, 2, 3
- [8] Rishabh Dabral, Muhammad Hamza Mughal, Vladislav Golyanik, and Christian Theobalt. Mofusion: A framework for denoising-diffusion-based motion synthesis. In *Computer Vision and Pattern Recognition (CVPR)*, 2023. 1, 2
- [9] Wenxun Dai, Ling-Hao Chen, Yufei Huo, Jingbo Wang, Jinpeng Liu, Bo Dai, and Yansong Tang. Motionlcm-v2: Improved compression rate for multi-latent-token diffusion, 2024. 2, 4, 3
- [10] Wenxun Dai, Ling-Hao Chen, Jingbo Wang, Jinpeng Liu, Bo Dai, and Yansong Tang. Motionlcm: Real-time controllable motion generation via latent consistency model. *arXiv preprint arXiv:2404.19759*, 2024. 2
- [11] Stefan Elfving, Eiji Uchibe, and Kenji Doya. Sigmoid-weighted linear units for neural network function approximation in reinforcement learning. *Neural networks*, 107: 3–11, 2018. 1
- [12] Lijie Fan, Tianhong Li, Siyang Qin, Yuanzhen Li, Chen Sun, Michael Rubinstein, Deqing Sun, Kaiming He, and Yonglong Tian. Fluid: Scaling autoregressive text-to-image generative models with continuous tokens. *arXiv preprint arXiv:2410.13863*, 2024. 5
- [13] Anindita Ghosh, Rishabh Dabral, Vladislav Golyanik, Christian Theobalt, and Philipp Slusallek. Remos: 3d motion-conditioned reaction synthesis for two-person interactions. In *European Conference on Computer Vision (ECCV)*, 2024. 1
- [14] Anindita Ghosh, Bing Zhou, Rishabh Dabral, Jian Wang, Vladislav Golyanik, Christian Theobalt, Philipp Slusallek, and Chuan Guo. Duetgen: Music driven two-person dance generation via hierarchical masked modeling. In *Proceedings of the Special Interest Group on Computer Graphics and Interactive Techniques Conference Conference Papers*, pages 1–11, 2025. 2
- [15] Chuan Guo, Xinxin Zuo, Sen Wang, Shihao Zou, Qingyao Sun, Annan Deng, Minglun Gong, and Li Cheng. Action2motion: Conditioned generation of 3d human motions. In *Proceedings of the 28th ACM International Conference on Multimedia*, pages 2021–2029, 2020. 5
- [16] Chuan Guo, Shihao Zou, Xinxin Zuo, Sen Wang, Wei Ji, Xingyu Li, and Li Cheng. Generating diverse and natural 3d human motions from text. In *Proceedings of the IEEE/CVF Conference on Computer Vision and Pattern Recognition (CVPR)*, 2022. 1, 2, 5, 3
- [17] Chuan Guo, Xinxin Zuo, Sen Wang, and Li Cheng. Tm2t: Stochastic and tokenized modeling for the reciprocal generation of 3d human motions and texts. In *ECCV*, 2022. 2
- [18] Chuan Guo, Yuxuan Mu, Muhammad Gohar Javed, Sen Wang, and Li Cheng. Momask: Generative masked modeling of 3d human motions. In *Proceedings of the IEEE/CVF Conference on Computer Vision and Pattern Recognition*, pages 1900–1910, 2024. 2, 3, 4, 8
- [19] Chuan Guo, Inwoo Hwang, Jian Wang, and Bing Zhou. Snapmogen: Human motion generation from expressive texts. *arXiv preprint arXiv:2507.09122*, 2025. 2, 3, 4
- [20] Martin Heusel, Hubert Ramsauer, Thomas Unterthiner, Bernhard Nessler, and Sepp Hochreiter. Gans trained by a two time-scale update rule converge to a local nash equilibrium. *Advances in neural information processing systems*, 30, 2017. 2
- [21] Fangzhou Hong, Vladimir Guзов, Hyo Jin Kim, Yuting Ye, Richard Newcombe, Ziwei Liu, and Lingni Ma. EgoIm: Multi-modal language model of egocentric motions. *arXiv preprint arXiv:2409.18127*, 2024. 2

- [22] Yiheng Huang, Hui Yang, Chuanchen Luo, Yuxi Wang, Shibo Xu, Zhaoxiang Zhang, Man Zhang, and Junran Peng. Stablemofusion: Towards robust and efficient diffusion-based motion generation framework. In *Proceedings of the 32nd ACM International Conference on Multimedia*, pages 224–232, 2024. 1
- [23] Muhammad Gohar Javed, Chuan Guo, Li Cheng, and Xingyu Li. Intermask: 3d human interaction generation via collaborative masked modelling. *arXiv preprint arXiv:2410.10010*, 2024. 2
- [24] Biao Jiang, Xin Chen, Wen Liu, Jingyi Yu, Gang Yu, and Tao Chen. Motiongpt: Human motion as a foreign language. *Advances in Neural Information Processing Systems*, 36, 2024. 2, 3
- [25] Lei Jiang, Ye Wei, and Hao Ni. Motionpcm: Real-time motion synthesis with phased consistency model. *arXiv preprint arXiv:2501.19083*, 2025. 2
- [26] Korrawe Karunratanakul, Konpat Preechakul, Supasorn Suwanajakorn, and Siyu Tang. Guided motion diffusion for controllable human motion synthesis. In *Proceedings of the IEEE/CVF International Conference on Computer Vision*, pages 2151–2162, 2023. 1, 2
- [27] Junho Lee, Jeongwoo Shin, Hyungwook Choi, and Joonseok Lee. Latent diffusion models with masked autoencoders. In *Proceedings of the IEEE/CVF International Conference on Computer Vision*, pages 17422–17431, 2025. 3
- [28] Xingjian Leng, Jaskirat Singh, Yunzhong Hou, Zhenchang Xing, Saining Xie, and Liang Zheng. Repa-e: Unlocking vae for end-to-end tuning with latent diffusion transformers. *arXiv preprint arXiv:2504.10483*, 2025. 2, 3
- [29] Chuqiao Li, Julian Chibane, Yannan He, Naama Pearl, Andreas Geiger, and Gerard Pons-Moll. Unimotion: Unifying 3d human motion synthesis and understanding. *arXiv preprint arXiv:2409.15904*, 2024. 1, 2, 3
- [30] Tianhong Li, Yonglong Tian, He Li, Mingyang Deng, and Kaiming He. Autoregressive image generation without vector quantization. In *Advances in Neural Information Processing Systems*, 2024. 2, 5
- [31] Han Liang, Wenqian Zhang, Wenxuan Li, Jingyi Yu, and Lan Xu. Intergen: Diffusion-based multi-human motion generation under complex interactions. *International Journal of Computer Vision*, pages 1–21, 2024. 1, 2
- [32] Hung Yu Ling, Fabio Zinno, George Cheng, and Michiel Van De Panne. Character controllers using motion vaes. *ACM Trans. Graph.*, 2020. 2
- [33] Pinxin Liu, Luchuan Song, Junhua Huang, Haiyang Liu, and Chenliang Xu. Gesturelsm: Latent shortcut based co-speech gesture generation with spatial-temporal modeling. *arXiv preprint arXiv:2501.18898*, 2025. 2
- [34] Xingchao Liu, Chengyue Gong, and Qiang Liu. Flow straight and fast: Learning to generate and transfer data with rectified flow. *arXiv preprint arXiv:2209.03003*, 2022. 3, 5
- [35] Matthew Loper, Naureen Mahmood, Javier Romero, Gerard Pons-Moll, and Michael J. Black. SMPL: A skinned multi-person linear model. *ACM Trans. Graphics (Proc. SIGGRAPH Asia)*, 34, 2015. 6
- [36] Zhengyi Luo, Jinkun Cao, Kris Kitani, Weipeng Xu, et al. Perpetual humanoid control for real-time simulated avatars. In *Proceedings of the IEEE/CVF International Conference on Computer Vision*, pages 10895–10904, 2023. 2
- [37] Naureen Mahmood, Nima Ghorbani, Nikolaus F. Troje, Gerard Pons-Moll, and Michael J. Black. AMASS: archive of motion capture as surface shapes. In *IEEE/CVF International Conference on Computer Vision, ICCV*, 2019. 1, 2, 3, 5
- [38] Viktor Makoviychuk, Lukasz Wawrzyniak, Yunrong Guo, Michelle Lu, Kier Storey, Miles Macklin, David Hoeller, Nikita Rudin, Arthur Allshire, Ankur Handa, et al. Isaac gym: High performance gpu-based physics simulation for robot learning. *arXiv preprint arXiv:2108.10470*, 2021. 2
- [39] Zichong Meng, Yiming Xie, Xiaogang Peng, Zeyu Han, and Huaizu Jiang. Rethinking diffusion for text-driven human motion generation. *arXiv preprint arXiv:2411.16575*, 2024. 2, 3, 4, 5, 6, 7, 1
- [40] Zichong Meng, Zeyu Han, Xiaogang Peng, Yiming Xie, and Huaizu Jiang. Absolute coordinates make motion generation easy. *arXiv preprint arXiv:2505.19377*, 2025. 2, 4, 6, 7, 3
- [41] Zhikang Niu, Shujie Hu, Jeongsoo Choi, Yushen Chen, Peining Chen, Pengcheng Zhu, Yunting Yang, Bowen Zhang, Jian Zhao, Chunhui Wang, et al. Semantic-vae: Semantic-alignment latent representation for better speech synthesis. *arXiv preprint arXiv:2509.22167*, 2025. 3
- [42] Mathis Petrovich, Michael J. Black, and Gül Varol. TMR: Text-to-motion retrieval using contrastive 3D human motion synthesis. In *International Conference on Computer Vision (ICCV)*, 2023. 2, 3, 7, 1
- [43] Mathis Petrovich, Or Litany, Umar Iqbal, Michael J Black, Gül Varol, Xue Bin Peng, and Davis Rempe. Stmc: Multi-track timeline control for text-driven 3d human motion generation. *arXiv preprint arXiv:2401.08559*, 2024. 2, 3
- [44] Ekkasit Pinyoanuntapong, Muhammad Usama Saleem, Pu Wang, Minwoo Lee, Srijan Das, and Chen Chen. Bamm: bidirectional autoregressive motion model. In *European Conference on Computer Vision*, pages 172–190. Springer, 2024. 2, 3, 4
- [45] Ekkasit Pinyoanuntapong, Pu Wang, Minwoo Lee, and Chen Chen. Mmm: Generative masked motion model. In *Proceedings of the IEEE/CVF Conference on Computer Vision and Pattern Recognition (CVPR)*, 2024. 2, 3, 4
- [46] Ekkasit Pinyoanuntapong, Muhammad Saleem, Korrawe Karunratanakul, Pu Wang, Hongfei Xue, Chen Chen, Chuan Guo, Junli Cao, Jian Ren, and Sergey Tulyakov. Maskcontrol: Spatio-temporal control for masked motion synthesis. In *Proceedings of the IEEE/CVF International Conference on Computer Vision*, pages 9955–9965, 2025. 2
- [47] Matthias Plappert, Christian Mandery, and Tamim Asfour. The kit motion-language dataset. *Big data*, 4(4):236–252, 2016. 1
- [48] Abhinanda R. Punnakkal, Arjun Chandrasekaran, Nikos Athanasiou, Alejandra Quiros-Ramirez, and Michael J. Black. BABEL: Bodies, action and behavior with english labels. In *Proceedings IEEE/CVF Conf. on Computer Vision and Pattern Recognition (CVPR)*, 2021. 4, 5
- [49] Alec Radford, Jong Wook Kim, Chris Hallacy, Aditya Ramesh, Gabriel Goh, Sandhini Agarwal, Girish Sastry, Amanda Askell, Pamela Mishkin, Jack Clark, Gretchen

- Krueger, and Ilya Sutskever. Learning transferable visual models from natural language supervision, 2021. 2
- [50] Colin Raffel, Noam Shazeer, Adam Roberts, Katherine Lee, Sharan Narang, Michael Matena, Yanqi Zhou, Wei Li, and Peter J Liu. Exploring the limits of transfer learning with a unified text-to-text transformer. *Journal of machine learning research*, 21(140):1–67, 2020. 5
- [51] Davis Remppe, Tolga Birdal, Aaron Hertzmann, Jimei Yang, Srinath Sridhar, and Leonidas J Guibas. Humor: 3d human motion model for robust pose estimation. In *Proceedings of the IEEE/CVF international conference on computer vision*, pages 11488–11499, 2021. 2
- [52] Yoni Shafir, Guy Tevet, Roy Kapon, and Amit Haim Bermano. Priormdm: Human motion diffusion as a generative prior. In *ICLR*, 2023. 2
- [53] Guy Tevet, Sigal Raab, Brian Gordon, Yoni Shafir, Daniel Cohen-or, and Amit Haim Bermano. Human motion diffusion model. In *The Eleventh International Conference on Learning Representations*, 2023. 1, 2, 4, 3
- [54] Emanuel Todorov, Tom Erez, and Yuval Tassa. Mujoco: A physics engine for model-based control. In *2012 IEEE/RSJ international conference on intelligent robots and systems*, pages 5026–5033. IEEE, 2012. 2
- [55] Linnan Tu, Lingwei Meng, Zongyi Li, Hefei Ling, and Shijuan Huang. Autoregressive motion generation with gaussian mixture-guided latent sampling. In *The Thirty-ninth Annual Conference on Neural Information Processing Systems*. 2
- [56] Ashish Vaswani, Noam Shazeer, Niki Parmar, Jakob Uszkoreit, Llion Jones, Aidan N Gomez, Łukasz Kaiser, and Illia Polosukhin. Attention is all you need. *Advances in neural information processing systems*, 30, 2017. 1
- [57] Jordan Voas, Yili Wang, Qixing Huang, and Raymond Mooney. What is the best automated metric for text to motion generation? In *SIGGRAPH Asia 2023 Conference Papers*, pages 1–11, 2023. 2
- [58] Weilin Wan, Zhiyang Dou, Taku Komura, Wenping Wang, Dinesh Jayaraman, and Lingjie Liu. Tlcontrol: Trajectory and language control for human motion synthesis. In *European Conference on Computer Vision*, pages 37–54. Springer, 2024. 2
- [59] Haoru Wang, Wentao Zhu, Luyi Miao, Yishu Xu, Feng Gao, Qi Tian, and Yizhou Wang. Aligning motion generation with human perceptions. In *International Conference on Learning Representations (ICLR)*, 2025. 2
- [60] Yilin Wang, chuan guo, Yuxuan Mu, Muhammad Gohar Javed, Xinxin Zuo, Juwei Lu, Hai Jiang, and Li cheng. Motiondreamer: One-to-many motion synthesis with localized generative masked transformer. In *The Thirteenth International Conference on Learning Representations*, 2025. 2
- [61] Ge Wu, Shen Zhang, Ruijing Shi, Shanghua Gao, Zhenyuan Chen, Lei Wang, Zhaowei Chen, Hongcheng Gao, Yao Tang, Jian Yang, et al. Representation entanglement for generation: Training diffusion transformers is much easier than you think. *arXiv preprint arXiv:2507.01467*, 2025. 2, 3
- [62] Lixing Xiao, Shunlin Lu, Huaijin Pi, Ke Fan, Liang Pan, Yueer Zhou, Ziyong Feng, Xiaowei Zhou, Sida Peng, and Jingbo Wang. Motionstreamer: Streaming motion generation via diffusion-based autoregressive model in causal latent space. *arXiv preprint arXiv:2503.15451*, 2025. 2, 3, 4, 5, 6, 7, 8, 1
- [63] Sihyun Yu, Sangkyung Kwak, Huiwon Jang, Jongheon Jeong, Jonathan Huang, Jinwoo Shin, and Saining Xie. Representation alignment for generation: Training diffusion transformers is easier than you think. In *International Conference on Learning Representations*, 2025. 2, 3
- [64] Zhengdi Yu, Simone Foti, Linguang Zhang, Amy Zhao, Cem Keskin, Stefanos Zafeiriou, and Tolga Birdal. Geometric neural distance fields for learning human motion priors. *arXiv preprint arXiv:2509.09667*, 2025. 2
- [65] Weihao Yuan, Yisheng He, Weichao Shen, Yuan Dong, Xiaodong Gu, Zilong Dong, Liefeng Bo, and Qixing Huang. Mogents: Motion generation based on spatial-temporal joint modeling. *Advances in Neural Information Processing Systems*, 37:130739–130763, 2024. 4, 3
- [66] Jianrong Zhang, Yangsong Zhang, Xiaodong Cun, Shaoli Huang, Yong Zhang, Hongwei Zhao, Hongtao Lu, and Xi Shen. T2m-gpt: Generating human motion from textual descriptions with discrete representations. In *Proceedings of the IEEE/CVF Conference on Computer Vision and Pattern Recognition (CVPR)*, 2023. 2, 3
- [67] Mingyuan Zhang, Zhongang Cai, Liang Pan, Fangzhou Hong, Xinying Guo, Lei Yang, and Ziwei Liu. Motiondiffuse: Text-driven human motion generation with diffusion model. *arXiv preprint arXiv:2208.15001*, 2022. 1, 2
- [68] Mingyuan Zhang, Xinying Guo, Liang Pan, Zhongang Cai, Fangzhou Hong, Huirong Li, Lei Yang, and Ziwei Liu. Remodiffuse: Retrieval-augmented motion diffusion model. *arXiv preprint arXiv:2304.01116*, 2023. 1
- [69] Mingyuan Zhang, Huirong Li, Zhongang Cai, Jiawei Ren, Lei Yang, and Ziwei Liu. Finemogen: Fine-grained spatio-temporal motion generation and editing. *NeurIPS*, 36, 2024.
- [70] Mingyuan Zhang, Daisheng Jin, Chenyang Gu, Fangzhou Hong, Zhongang Cai, Jingfang Huang, Chongzhi Zhang, Xinying Guo, Lei Yang, Ying He, et al. Large motion model for unified multi-modal motion generation. In *European Conference on Computer Vision*, pages 397–421. Springer, 2025. 2
- [71] Pengfei Zhang, Pinxin Liu, Pablo Garrido, Hyeonwoo Kim, and Bindita Chaudhuri. Kinmo: Kinematic-aware human motion understanding and generation. In *Proceedings of the IEEE/CVF International Conference on Computer Vision*, pages 11187–11197, 2025. 2
- [72] Zeyu Zhang, Yiran Wang, Danning Li, Dong Gong, Ian Reid, and Richard Hartley. Flashmo: Geometric interpolants and frequency-aware sparsity for scalable efficient motion generation. In *The Thirty-ninth Annual Conference on Neural Information Processing Systems*. 2
- [73] Zeyu Zhang, Akide Liu, Ian Reid, Richard Hartley, Bohan Zhuang, and Hao Tang. Motion mamba: Efficient and long sequence motion generation with hierarchical and bidirectional selective ssm. *arXiv preprint arXiv:2403.07487*, 2024. 2
- [74] Kaifeng Zhao, Gen Li, and Siyu Tang. A diffusion-based autoregressive motion model for real-time text-driven motion control. In *The Thirteenth International Conference on Learning Representations (ICLR 2025)*, 2025. 2

- [75] Wenyang Zhou, Zhiyang Dou, Zeyu Cao, Zhouyingcheng Liao, Jingbo Wang, Wenjia Wang, Yuan Liu, Taku Komura, Wenping Wang, and Lingjie Liu. Emdm: Efficient motion diffusion model for fast, high-quality motion generation. *arXiv preprint arXiv:2312.02256*, 2023. [1](#), [2](#)
- [76] Bingfan Zhu, Biao Jiang, Sunyi Wang, Shixiang Tang, Tao Chen, Linjie Luo, Youyi Zheng, and Xin Chen. Motiongpt3: Human motion as a second modality. *arXiv preprint arXiv:2506.24086*, 2025. [2](#), [3](#)



# MoLingo: Motion–Language Alignment for Text-to-Human Motion Generation

## Supplementary Material

Table 4. **Notation Table.** The main notation used in our paper.

Symbol	Description	Domain
$N$	Input motion sequence length	$\mathbb{N}$
$D$	Pose configuration dimension	$\mathbb{N}$
$l$	Motion latent length	$\mathbb{N}$
$d$	Latent dimension	$\mathbb{N}$
$D_h$	Hidden size of Transformer decoder	$\mathbb{N}$
$l_{\text{adapter}}$	Text adapter depth	$\mathbb{N}$
$l_{\text{text}}$	Text token length for cross attention	$\mathbb{N}$
$\tau$	Threshold for filtering repetitive class tokens	$\mathbb{N}$
$\mathbf{m}$	Input motion sequence	$\mathbb{R}^{N \times D}$
$m$	Motion latent sequence	$\mathbb{R}^{l \times d}$
$\kappa$	Class token sequence	$\mathbb{R}^{l \times d}$
$\mathcal{I}$	Index set of chosen positions for $\mathcal{L}_{\text{sem}}$	-
$\mathbf{w}$	Text representation for cross attention	$\mathbb{R}^{l_{\text{text}} \times D_h}$
$\mathcal{E}$	Encoder	-
$\mathcal{D}$	Decoder	-
$v_\theta$	Rectified flow MLP	-

In this supplementary document, we first present additional implementation details, including autoencoder training, the auto-regressive denoising model, integration with the RL tracking controller, and the evaluation metrics. Next, we report further quantitative results, such as effect of text adapter, comparisons with MotionStreamer [62] and a broader set of benchmarks under the TMR-263 [42] evaluation protocol. Finally, we include an ablation study that highlights the impact of our repetitive class-token filtering design during SAE training. The main notation used in our paper is shown in Tab. 4.

## 6. More Implementation Details

**Autoencoder training.** We adopt the causal autoencoder architecture from [62] with a hidden size of 1024, and provide a detailed specification in Tab. 9. Unlike [62], we address an issue happening when the 1D convolutional kernel slides from the beginning to the end of the motion sequence: kernels at the start of the sequence encounter padded values (set to 0 in previous works), which leads to jitter in the decoded motion during the first few frames. To mitigate this, for the first convolutional layer of the encoder, we replace zero padding with replicated padding, resulting in more stable training and smoother reconstructions. Tab. 7 shows our SAE achieves lower reconstruction FID (rFID) while maintaining comparable MPJPE compared with MotionStreamer [62]’s VAE. In practice, we set  $\lambda_{\text{joint}} = 1.0$  and  $\lambda_{\text{vel}} = 10.0$ . For both the VAE and SAE, we use  $\lambda_{\text{KL}} = 1 \times 10^{-5}$ . For the SAE, based on the ablation results in Tab. 3, we set  $\lambda_{\text{sem}} = 0.001$ . The threshold  $\tau$  for filtering repetitive class

Table 5. **Effect of text adapter depth.** We compare models without a text adapter and with text adapters of different depths (3, 6, and 9 layers). Using a 6-layer adapter (ours) gives the best overall trade-off, improving FID and R-Precision across all others. We conduct all experiments on MARDM-67 [39] evaluator using a VAE with a downsampling 4 $\times$  and latent dimension 16.

Configuration	FID $\downarrow$	R-Precision $\uparrow$		
		Top 1	Top 2	Top 3
w/o text adapter	0.057 $\pm$ .001	0.524 $\pm$ .003	0.715 $\pm$ .001	0.810 $\pm$ .002
depth=3	0.060 $\pm$ .002	0.521 $\pm$ .002	0.713 $\pm$ .002	0.807 $\pm$ .002
depth=6 (Ours)	0.049 $\pm$ .003	0.528 $\pm$ .002	0.721 $\pm$ .002	0.815 $\pm$ .002
depth=9	0.053 $\pm$ .002	0.527 $\pm$ .002	0.719 $\pm$ .002	0.813 $\pm$ .001

Table 6. **Effect of repetitive class token filtering.** We ablate generative performance with and without repetitive class token filtering during SAE training. Filtering consistently improves FID and retrieval scores, indicating that it acts as a soft semantic regularizer, encouraging coherence without forcing adjacent motion latents to collapse to the same text label.

Configuration	FID $\downarrow$	R-Precision $\uparrow$		
		Top 1	Top 2	Top 3
w/o filtering	0.096 $\pm$ .003	0.524 $\pm$ .002	0.713 $\pm$ .002	0.811 $\pm$ .002
w/ filtering (Ours)	0.064 $\pm$ .002	0.542 $\pm$ .002	0.739 $\pm$ .002	0.832 $\pm$ .002

token is set to 0.995.

**Obtaining text labels for a specific motion latent.** During SAE training, to obtain text labels that are temporally aligned with a given motion latent  $m_i$ , we exploit the causal design: each latent depends only on past frames, not future ones. As shown in Tab. 9, our encoder comprises four causal 1D convolutional layers in total (excluding the ResNet layers). The first and last layers use a kernel size of 3 and stride of 1 to preserve the sequence length, while the two middle layers use a kernel size of 4 and stride of 2, each downsampling the temporal resolution by a factor of 2. This yields a latent sequence whose length is one quarter of the original. As a result, latent index  $i$  is influenced by the original frames from  $4i - 16$  to  $4i + 4$ , covering 20 frames in total. We aggregate the frame-level text labels over the same temporal window from  $4i - 16$  to  $4i + 4$ , encode them with T5-Large to obtain embeddings, and then take the average of these embeddings before feeding them into an MLP projection.

**Auto-regressive motion latent denoising.** Our Transformer for predicting  $z$  is a standard Transformer decoder [56] with 16 layers, each using 16 attention heads and a hidden size of  $D_h = 1024$ . For denoising, we use an MLP with 8 residual blocks and a width of 1280 channels. Each block applies LayerNorm, a linear layer, a SiLU [11] activation, and another linear layer, followed by a residual connection. The

MLP is conditioned on the  $z$  predicted by the Transformer: we add  $z$  to the time embedding of the noise-schedule step  $t$ , and use this combined signal to modulate the LayerNorm layers via AdaLN. We set  $l_{\text{text}} = 128$ . During inference, we use a stochastic sampler that, at each step, applies a small noise refresh, partially replacing the clean component with fresh prior noise. This maintains stochasticity and improves sample diversity compared to a purely deterministic ODE trajectory. To avoid confusion, we distinguish two terms. **Denosing step** is the number of denoising iterations for the reverse ODE process during denoising, whereas **inference step** is the number of auto-regressive iterations used to sample the motion latent sequence. In all experiments, we fix the denoising steps to 32 and set the number of inference step to 16 in practice. Motion generation takes an average of 2.83 seconds per sample when evaluated on the HumanML3D test set.

**User study interface.** The detailed instructions and interface layout of our user study are shown in Fig. 7. In each trial, we randomly select 15 samples and randomly assign them to the left or right side. We prepare three questionnaires with the same layout, each comparing our method against a different baseline. For comparison with MotionStreamer [62], we use the model trained with the 272D representation, and for comparisons with MoMask [18] and DisCoRD [7], we use the model trained with the 263D representation.

**Integrate MoLingo with RL tracking controller.** To make the generated motions more physically plausible, we integrate each generator with a pre-trained RL tracking controller. Specifically, we first re-train a PHC [36] policy for the Unitree G1 humanoid to track the joint positions of human motions. After generating motions with each candidate generator, we retarget them to the humanoid’s body shape and then directly deploy the tracking policy to assess performance. Because the 272D representation contains valid rotational components, retargeting is more convenient; thus, we conduct this evaluation using the 272D model and compare against MotionStreamer. The policy is trained in Isaac-Gym [38] with 2048 parallel environments. After obtaining the generated motions, we first retarget them to match G1’s morphology and extract the corresponding joint position sequences. These joint positions are then provided to the policy to roll out action trajectories. Finally, we replay the resulting actions in the MuJoCo [54] for visualization. Video comparisons are available on our local webpage.

**Details of evaluation metrics.** We use the evaluation metrics following [16, 39, 62]: (1) **Fréchet Inception Distance (FID)** quantifies how close the generated motions are to real ones by comparing the overall distributions of predicted and ground-truth motion sequences, by applying a pre-trained feature extractor for both motion and text. (2) **R-Precision** (Top-1/Top-2/Top-3) together with Matching-score evaluates

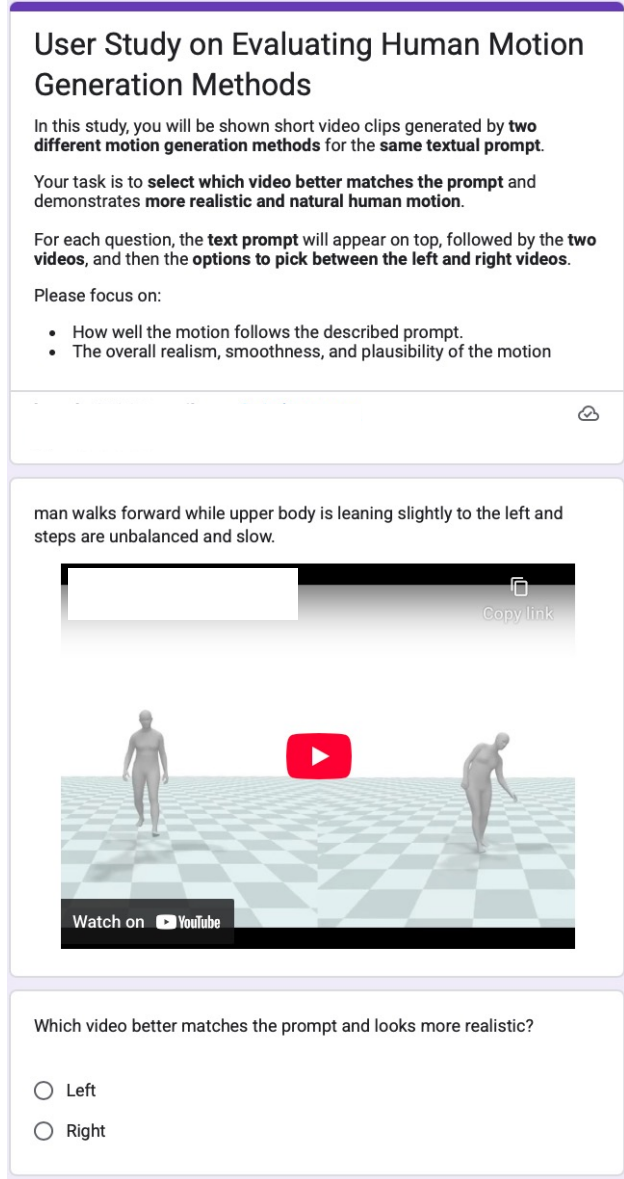


Figure 7. User study interface.

text–motion consistency by checking whether generated motion embeddings retrieve their paired text prompts among the top candidates. (3) **MultiModality** (MModality) reflects variation under identical prompts, measuring how diverse the produced motion embeddings are when generating multiple motions for the same text. (4) **CLIP-Score** measures textual faithfulness via CLIP [49], computed as the cosine similarity between CLIP embeddings of the generated motion and its text description.

## 7. More Quantitative Results

**Effect of the text adapter.** Tab. 5 reports an ablation over different numbers of text adapter layers. Using the adapter im-

Table 7. **Quantitative comparison with MotionStreamer.** MotionStreamer proposed a TMR-style [42] feature extractor used as an evaluator in their own 272D representation. To ensure a fair comparison, we train our model on the 272D HumanML3D data and evaluate using their evaluator. rFID denotes reconstruction FID, and MPJPE is measured in millimeters. Our replicated padding design improves reconstruction realism in terms of rFID while preserving comparable MPJPE. For generation, our method achieves significant improvements over MotionStreamer across all metrics. We run the experiment 20 runs and  $\pm$  indicates 95% confidence interval. We apply  $4\times$  downsampling and latent dimension 16 with a well-trained SAE.

Methods	rFID $\downarrow$	MPJPE $\downarrow$	FID $\downarrow$	R-Precision			Matching Score $\downarrow$
				Top 1 $\uparrow$	Top 2 $\uparrow$	Top 3 $\uparrow$	
Real	0.000	0.000	$0.002^{\pm.000}$	$0.702^{\pm.000}$	$0.864^{\pm.000}$	$0.914^{\pm.000}$	$15.151^{\pm.000}$
MotionStreamer [62]	0.661	22.90	$11.979^{\pm.078}$	$0.629^{\pm.004}$	$0.791^{\pm.003}$	$0.858^{\pm.003}$	$16.019^{\pm.017}$
MoLingo (Ours)	0.280	23.01	$3.444^{\pm.035}$	$0.788^{\pm.001}$	$0.912^{\pm.002}$	$0.950^{\pm.001}$	$14.591^{\pm.017}$

Table 8. **Quantitative results on the TMR-263 evaluator.** We compare our method with a broad set of motion generation approaches, from early models [6, 53] to recent ones [7, 76], covering pose-frame diffusion [53], single-vector latent diffusion [6, 9], VQ-based next-token prediction [7, 18, 19, 44, 45, 65], and continuous-valued auto-regressive models [76]. We report the mean results over 20 independent runs, and the  $\pm$  values indicate the 95% confidence interval. We do not compare with MARDM [39] and ACMDM [40] here because of the motion representation inconsistency. Our method achieves state-of-the-art FID, R-Precision, and MultiModality. Green cells highlight the best scores, and yellow cells the second best.

Methods	FID $\downarrow$	R-Precision			MModality $\uparrow$
		Top 1 $\uparrow$	Top 2 $\uparrow$	Top 3 $\uparrow$	
Real	$0.000^{\pm.000}$	$0.676^{\pm.002}$	$0.810^{\pm.002}$	$0.861^{\pm.002}$	-
MDM-50Step [53]	$0.093^{\pm.000}$	$0.563^{\pm.007}$	$0.723^{\pm.007}$	$0.794^{\pm.006}$	$34.207^{\pm.598}$
MLD [6]	$0.052^{\pm.000}$	$0.579^{\pm.006}$	$0.729^{\pm.007}$	$0.797^{\pm.004}$	$32.481^{\pm.678}$
MoMask [18]	$0.022^{\pm.000}$	$0.687^{\pm.002}$	$0.825^{\pm.002}$	$0.877^{\pm.002}$	$18.406^{\pm.583}$
MMM [45]	$0.024^{\pm.000}$	$0.710^{\pm.002}$	$0.834^{\pm.002}$	$0.881^{\pm.001}$	$15.286^{\pm.577}$
BAMM [44]	$0.044^{\pm.000}$	$0.652^{\pm.002}$	$0.790^{\pm.002}$	$0.845^{\pm.002}$	$28.703^{\pm.672}$
MogenTS [65]	$0.017^{\pm.000}$	$0.687^{\pm.003}$	$0.819^{\pm.002}$	$0.870^{\pm.002}$	$12.102^{\pm.394}$
MLD++ [9]	$0.019^{\pm.000}$	$0.736^{\pm.003}$	$0.863^{\pm.002}$	$0.907^{\pm.002}$	$26.515^{\pm.621}$
MotionLCM-V2 [9]	$0.026^{\pm.000}$	$0.751^{\pm.003}$	$0.879^{\pm.001}$	$0.921^{\pm.001}$	$28.424^{\pm.753}$
DisCoRD [7]	$0.020^{\pm.000}$	$0.692^{\pm.002}$	$0.828^{\pm.002}$	$0.878^{\pm.001}$	$18.804^{\pm.613}$
MotionGPT3 [76]	$0.021^{\pm.000}$	$0.758^{\pm.002}$	$0.873^{\pm.002}$	$0.915^{\pm.001}$	$20.821^{\pm.426}$
MoMask++ [19]	$0.020^{\pm.000}$	$0.692^{\pm.003}$	$0.824^{\pm.002}$	$0.874^{\pm.002}$	$16.589^{\pm.439}$
MoLingo	$0.014^{\pm.000}$	$0.772^{\pm.003}$	$0.889^{\pm.002}$	$0.928^{\pm.002}$	$21.235^{\pm.519}$

proves generative performance in both FID and R-Precision compared to not using it, as it strengthens text–motion communication during training. We select a depth of 6 layers, which yields the best performance.

**Comparison with MotionStreamer.** To ensure a fair comparison, we use the evaluator from [62], trained on the HumanML3D-272 dataset with the TMR contrastive strategy. We compare FID, R-Precision, and Matching Score as reported under MotionStreamer’s original evaluation setting. As shown in Tab. 7, Molingo achieves significant improvements on all metrics. We apply CFG scale 7.0 for 272D format generation. The experiment is conducted with HumanML3D-272 test set.

**Quantitative results on the TMR-263 evaluator [42].** We

further provide, for the first time, a benchmark evaluating a broad set of methods on the TMR-263 evaluator. TMR is trained with an improved contrastive loss, yielding a better cross-modal embedding space. We rerun a wide range of baseline methods on this evaluator, as shown in Tab. 8, Molingo still achieves state-of-the-art performance across all methods. The experiment is conducted with HumanML3D [16] test set.

**Effect of repetitive token filtering.** During SAE training, to ablate the effect of repetitive class-token filtering, Tab. 6 reports the generative performance with and without filtering. Removing adjacent repetitive class tokens acts as a softer regularizer and yields significantly better performance.

Table 9. **Detail architecture** of our autoencoders. Different from [62], we set the padding mode of the first 1D convolutional layer to replicate the initial frames, which stabilizes training and improves reconstruction.

Components	Architecture
Encoder	<p>(0): CausalConv1D(<math>D</math>, 1024, kernel_size=(3,), stride=(1,), dilation=(1,), padding=((2,), mode=replicate))</p> <p>(1): SiLU()</p> <p>(2): <math>2 \times</math> Sequential(            (0): CausalConv1D(1024, 1024, kernel_size=(4,), stride=(2,), dilation=(1,), padding=((2,), mode=zero))            (1): CausalResnet1D(              (0): CausalResConv1DBlock(                (activation1): SiLU()                (conv1): CausalConv1D(1024, 1024, kernel_size=(3,), stride=(1,), dilation=(9,), padding=((18,), mode=zero))                (activation2): SiLU()                (conv2): CausalConv1D(1024, 1024, kernel_size=(1,), stride=(1,), dilation=(1,), padding=((0,), mode=zero))              (1): CausalResConv1DBlock(                (activation1): SiLU()                (conv1): CausalConv1D(1024, 1024, kernel_size=(3,), stride=(1,), dilation=(3,), padding=((6,), mode=zero))                (activation2): SiLU()                (conv2): CausalConv1D(1024, 1024, kernel_size=(1,), stride=(1,), dilation=(1,), padding=((0,), mode=zero))              (2): CausalResConv1DBlock(                (activation1): SiLU()                (conv1): CausalConv1D(1024, 1024, kernel_size=(3,), stride=(1,), dilation=(1,), padding=((2,), mode=zero))                (activation2): SiLU()                (conv2): CausalConv1D(1024, 1024, kernel_size=(1,), stride=(1,), dilation=(1,), padding=((0,), mode=zero))))            (3): CausalConv1D(1024, 1024, kernel_size=(3,), stride=(1,), dilation=(1,), padding=((2,), mode=zero))</p>
Decoder	<p>(0): CausalConv1D(<math>d</math>, 1024, kernel_size=(3,), stride=(1,), dilation=(1,), padding=((2,), mode=zero))</p> <p>(1): SiLU()</p> <p>(2): <math>2 \times</math> Sequential(            (0): CausalResnet1D(              (0): CausalResConv1DBlock(                (activation1): SiLU()                (conv1): CausalConv1D(1024, 1024, kernel_size=(3,), stride=(1,), dilation=(9,), padding=((18,), mode=zero))                (activation2): SiLU()                (conv2): CausalConv1D(1024, 1024, kernel_size=(1,), stride=(1,), dilation=(1,), padding=((0,), mode=zero))              (1): CausalResConv1DBlock(                (activation1): SiLU()                (conv1): CausalConv1D(1024, 1024, kernel_size=(3,), stride=(1,), dilation=(3,), padding=((6,), mode=zero))                (activation2): SiLU()                (conv2): CausalConv1D(1024, 1024, kernel_size=(1,), stride=(1,), dilation=(1,), padding=((0,), mode=zero))              (2): CausalResConv1DBlock(                (activation1): SiLU()                (conv1): CausalConv1D(1024, 1024, kernel_size=(3,), stride=(1,), dilation=(1,), padding=((2,), mode=zero))                (activation2): SiLU()                (conv2): CausalConv1D(1024, 1024, kernel_size=(1,), stride=(1,), dilation=(1,), padding=((0,), mode=zero))))            (1): Upsample(scale_factor=2.0, mode=nearest)            (2): CausalConv1D(1024, 1024, kernel_size=(3,), stride=(1,), dilation=(1,), padding=((2,), mode=zero))            (3): CausalConv1D(1024, 1024, kernel_size=(3,), stride=(1,), dilation=(1,), padding=((2,), mode=zero))            (4): SiLU()            (5): CausalConv1D(1024, <math>D</math>, kernel_size=(3,), stride=(1,), dilation=(1,), padding=((2,), mode=zero))</p>
Autoencoder	<p>(0): Encoder(<math>D</math>, 1024)</p> <p>(1): MLP(1024, <math>d</math>)</p> <p>(2): Decoder(<math>d</math>, <math>D</math>)</p>